AIP | Review of Scientific Instruments

In situ multi-modal monitoring of solvent vapor swelling in polymer thin films

Dat Tien Hoang, Jaesung Yang, Keewook Paeng, Youngah Kwon, Oh Sang Kweon, and Laura J. Kaufman

Citation: Review of Scientific Instruments **87**, 015106 (2016); doi: 10.1063/1.4939669
View online: http://dx.doi.org/10.1063/1.4939669
View Table of Contents: http://scitation.aip.org/content/aip/journal/rsi/87/1?ver=pdfcov
Published by the AIP Publishing

REVIEW OF SCIENTIFIC INSTRUMENTS **87**, 015106 (2016)

In situ multi-modal monitoring of solvent vapor swelling in polymer thin films

Dat Tien Hoang,[1] Jaesung Yang,[1] Keewook Paeng,[1,2] Youngah Kwon,[1] Oh Sang Kweon,[1] and Laura J. Kaufman[1,a)]
[1]*Department of Chemistry, Columbia University, New York, New York 10027, USA*
[2]*Department of Chemistry, Sungkyunkwan University, Suwon 440-746, South Korea*

(Received 7 July 2015; accepted 26 December 2015; published online 12 January 2016)

Polymer processing techniques involving solvent vapor swelling are typically challenging to control and thus reproduce. Moreover, traditional descriptions of solvent swollen films lack microscopic detail. We describe the design and use of an apparatus that facilitates macroscopic and microscopic characterization of samples undergoing solvent vapor swelling in a controlled environment. The experimental design incorporates three critical characteristics: (1) a mass-flow controlled solvent vapor delivery system allows for precise control of the amount of solvent vapor delivered to the sample, (2) a sample prepared on a quartz crystal microbalance allows for real-time assessment of the extent of sample swelling, (3) a second sample prepared and assessed in parallel on a coverslip allows real-time fluorescence microscopy during swelling. We demonstrate that this apparatus allows for single-particle tracking, which in turn facilitates *in situ* monitoring of local environments within the solvent-swollen film. © *2016 AIP Publishing LLC.* [http://dx.doi.org/10.1063/1.4939669]

I. INTRODUCTION

Polymers in contact with a compatible liquid- or vapor-phase solvent undergo swelling. Homopolymer swelling has been extensively studied theoretically and experimentally, and polymer swelling behavior has been exploited for applications including photolithography and ion exchange.[1–5] In 1995, polymer swelling through exposure to solvent vapor was used as a tool for attaining long-range nanoscale ordering in diblock copolymer thin films in a process that became known as solvent vapor annealing (SVA).[6] This approach has become a widely used alternative to thermal annealing for attaining order in such materials, as it is typically both milder and more efficient than thermal annealing.[7,8] In recent years, there has been significant effort directed towards understanding and controlling the SVA process to attain better ordering in thin films of diblock copolymers as well as for bottom-up assembly of organic materials.[7,9] Despite this, SVA remains poorly understood and of limited reproducibility, with conditions set empirically for individual applications by individual laboratories.[7]

Polymer swelling is a complex phenomenon. In the homopolymer case, swelling comprises two competing phenomena, solvent diffusion through the polymer and relaxation of the polymer.[5] The relative rates of solvent diffusion and host relaxation determine the details of the solvent swelling process as well as the molecular rearrangements that occur upon swelling. For example, polymers in a thin film prepared by spin-coating have been shown to reptate following swelling with a good solvent.[10,11] When applied to diblock copolymers, the aforementioned complexities are exacerbated by phase segregation of the individual blocks into nanostructures.[7,12,13] While SVA clearly enhances the microphase segregation in these systems, allowing for long range order to be achieved, the ways in which solvent choice, vapor pressure, and degree and time course of swelling can be used to enhance and control this ordering remain unclear.

A key limitation to developing a fuller understanding of the SVA process is the limited capacity to monitor the process *in situ*. It is relatively straightforward to monitor degree of solvent uptake in a polymeric thin film via quartz crystal microbalances (QCMs) or optical metrology techniques.[4,5,14–18] QCMs operating in dissipation mode could additionally report bulk viscoelastic properties of a film during the process.[15] Evolving structural changes and potential inhomogeneity of structure and mechanical properties across the films over time are more challenging to assess during SVA. For diblock copolymers, grazing incidence small-angle x-ray scattering (GISAXS) has been used to assess transient nanostructures that arise during swelling.[12,13,19–22] While GISAXS can reveal nanostructural motifs present in a swollen film, it cannot describe molecular motions in a spatially resolved manner. Indeed, no study to date has simultaneously assessed film thickness and local structure or dynamics in real time. Moreover, most of the aforementioned studies did not quantitatively control solvent vapor pressure, limiting ability to reproduce findings and generalize results.

Here, we describe an apparatus for controlled delivery of solvent vapor to polymer thin film samples and simultaneous monitoring of multiple properties of those samples throughout the process of solvent vapor annealing. To achieve this multi-modal monitoring, two polymer thin films are prepared in an identical fashion and assessed in parallel adjacent to each other within a single sample chamber. One sample, prepared

a)Author to whom correspondence should be addressed. Electronic mail: kaufman@chem.columbia.edu

on a QCM, is used to characterize the extent of swelling while another, prepared on a coverslip, is used for epi-fluorescence imaging. Swelling is performed in a controlled fashion using a series of mass-flow controllers (MFCs) to generate and control solvent vapor pressures. This approach to studying polymer films in their vapor swollen state allows simultaneous characterization of film swelling, viscoelasticity, structure, and/or dynamics under well-controlled conditions.

We demonstrate the broad utility of information that can be accessed using this apparatus via two proof-of-principle experiments. In one case, the dynamics within a polymer thin film are characterized by particle-tracking quantum dot (QD) dopants, data that illuminate both bulk enhancement of diffusion that occurs upon swelling as well as heterogeneity in dynamics across the swollen film. In a second example, a mixture of solvents is used to monitor the aggregation of conjugated polymer guests, demonstrating that the control of the conditions in the sample chamber is sufficient to direct bottom-up assembly of mesoscopic structures.

II. APPARATUS

A. Solvent vapor annealing chamber

The sample chamber is composed of three parts—the base, the body, and the lid—machined from aluminum. Within the sample chamber, two polymer thin films were prepared and assessed in parallel, with a coverslip-mounted sample at the chamber base and a QCM-mounted sample at the chamber lid (Fig. 1). The base has an opening to hold a 25 mm diameter coverslip, sealed with Kalrez O-rings. The sample chamber lid is designed such that it can be fastened between the QCM crystal holder head and the retainer cover that holds the QCM in place (Fig. 1(c)). The QCM sensor lies above and concentric to the imaged sample. An inlet and outlet for vapor flow were bored through the sides of the cylinder body to allow connection to a MFC-regulated vapor flow system. The inlet and outlet to the sample chamber are controlled by two pin valves. The three components of the sample chamber are held together with bored-through screws with intercalating Kalrez O-rings to assure a good seal. In the experiments performed here, Teflon tape was applied around all junctures to further protect against possible leaks.

B. Solvent vapor production

Solvent vapor was generated using a series of mass-flow controllers (Alicat Scientific MCS-100) to bubble dry nitrogen carrier gas through solvent reservoirs. In the configuration shown in Fig. 2, two MFCs (MFC-A and MFC-B) control flow in two channels, though this system can be extended to more channels to support delivery of complex mixtures of solvents. A switch is present in each channel (S-A and S-B in Fig. 2) to allow bypassing of the solvent reservoir connected to that channel. The flow of each channel is combined in a mixing bottle to assure a reservoir of equilibrated vapor mixtures. Downstream from the mixing bottle, another switch (S-C) allows flow to or bypass of the sample chamber. Perfluoroalkoxy tubing (McMaster Carr; Ultraclear PFA Tubing, 1/8 in. inner diameter) was used to connect all the components involved with solvent vapor production and delivery since it is extremely resistant to a wide range of organic solvents.

C. Sample characterization

The sample at the bottom of the chamber was prepared on a coverslip and was interrogated via wide-field epi-fluorescence microscopy. The exemplary experiments described here employed continuous wave 488 nm excitation,

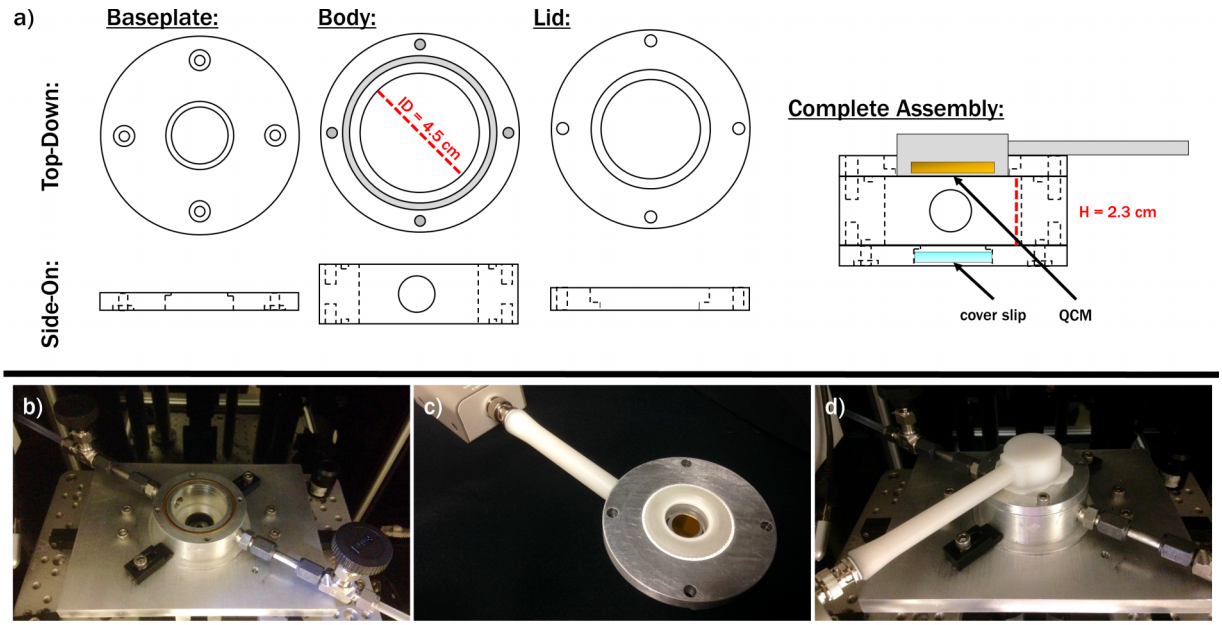

FIG. 1. (a) Schematic diagram of the chamber components both unassembled and assembled. (b)-(d) Photographs of the (b) sample chamber without lid, showing the coverslip in place over the objective lens, (c) underside of the chamber lid with the QCM attached, and (d) fully assembled chamber on the microscope sample stage.

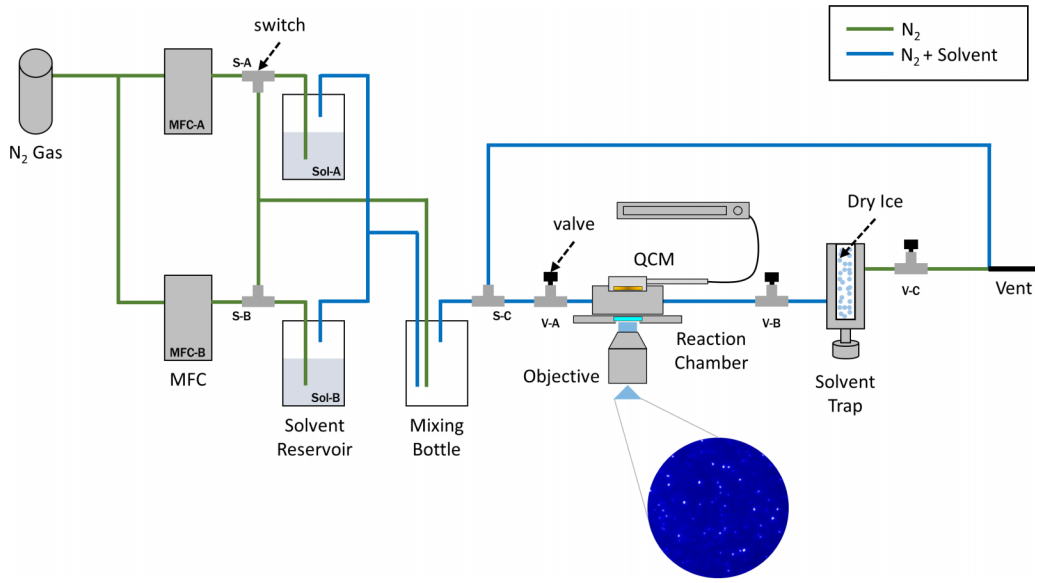

FIG. 2. Schematic diagram of the solvent vapor delivery system. MFCs control the flow of carrier gas through the appropriate solvent reservoirs and the sample chamber. Switches and valves are present throughout (indicated by S- and V-, respectively) to direct and control flow. The vent at right is left open except in cases where the solvent trap is used to condense solvent vapors to assess quantity of solvent that was delivered to the sample.

an oil-immersion objective lens (Olympus PlanApo N 60×, NA = 1.4), and appropriate dichroic (488 nm), longpass (520 nm), and bandpass (525-675 nm) filters. Images were collected using an EMCCD camera (Andor iXon DV-855).

In theory, the film employed for imaging could also be used to monitor film swelling through an optically based technique such as ellipsometry or interferometry. However, doing so could complicate fluorescence imaging; moreover, the film to be imaged must be prepared on a coverslip, which is not ideal for these approaches. Instead, film thickness and swelling were assessed via parallel measurements on a film prepared on the QCM (Stanford Research Systems QCM-200) at the sample chamber's top. This measurement does not interfere with imaging, and the QCM is compact and simple to operate. Moreover, the QCM can return information on film viscoelasticity that can be used to validate storage and loss moduli obtained, for example, via particle tracking microrheology on the coverslip-mounted film.[23] Film thickness before and during SVA was assessed by measuring the decrease in resonance frequency from a bare QCM to one with a spin-cast film prior to or during swelling. The change in QCM resonance frequency reports film uptake of solvent via the Sauerbrey equation,

$$\Delta f = -C_f \Delta m, \tag{1}$$

where Δf is the observed frequency change, C_f is the sensitivity factor for the crystal used, and Δm is the change of mass per area.[24] Change in mass per area can be transformed to film thickness (or change thereof) via

$$\Delta m = \rho \Delta h, \tag{2}$$

with ρ the density of the solvent responsible for the change in mass. To assure the (potentially evolving) viscoelasticity of the film does not affect measurement accuracy,[25] the QCM should be operated in a mode that corrects for resonance frequency changes due to viscoelastic losses.

III. CONTROL OF VAPOR PRESSURE

A. Single solvent delivery

As depicted in Fig. 2, solvent vapor was generated using MFCs to bubble dry nitrogen gas through solvent reservoirs. To assess the system's performance, expected and actual amounts of generated acetone vapor were compared.[14] The flow controllers allow direct control of Q, the volumetric flow rate. The following equation describes the relationship between volumetric and molar flow rate:

$$M = Q\rho/MW. \tag{3}$$

M is the molar flow rate, Q is the volumetric flow rate, ρ is the gas density, and MW is the molecular weight of the gas. For nitrogen gas, employing Q_{nit} = 100 standard cm^3/min (sccm) yields $M_{nit} = 4.147 \times 10^{-3}$ mol/min. At this flow condition, the Reynolds number in the tubing used is 177, indicating laminar flow.

To calculate the molar flow rate for the solvent vapor, several assumptions were made. First, it was assumed that bubbling nitrogen gas through a solvent promotes solvent evaporation, ensuring that solvent vapor pressure remains at saturation (p_{sol}) for a given temperature. Because the solubility of nitrogen in common solvents is negligible, it was also assumed that M_{nit} remains constant after bubbling. Finally, the total pressure in the system was assumed to be 760 Torr because the SVA is an open system with low flow rates. Given these assumptions, the molar flow rate for solvent vapor (M_{sol}) for a MFC-controlled channel is given by

$$M_{sol} = M_{nit}\left[\frac{p_{sol}}{760 - p_{sol}}\right]. \tag{4}$$

Since p_{ace} = 193.19 Torr at 21 °C, for Q_{nit} = 100 sccm, a volumetric flow rate of Q_{ace} = 93.51 μl/min was expected. Experimentally, over two trials, 1760 ± 110 μl acetone was recovered at the solvent trap when nitrogen gas flowed at Q_{nit} = 100 sccm for 20 min and bubbled through acetone. This volume corresponds to Q_{ace} = 88 ± 5 μl/min. With a deviation of less than 10% between predicted and measured recovered solvent, it was assumed there were no significant leaks present in the system.

In a single channel configuration such as that described above, altering M_{nit} will alter the rate of swelling, but the equilibrium vapor pressure in the chamber will be the saturated vapor pressure of the solvent regardless of M_{nit}. The film is thus expected to swell to the same degree over a range of nitrogen mass flow rates. To lower the vapor pressure of the delivered solvent relative to the saturated vapor pressure and decrease degree of film swelling, mass flow of nitrogen through the solvent can be lowered while keeping the total nitrogen mass flow rate identical by using the second MFC to deliver additional nitrogen gas to the chamber (bypassing the second solvent container). The vapor pressure at the sample is then given by

$$p = p_{sol} * M_{sol}/M_{nit,tot}, \quad (5)$$

where $M_{nit,tot}$ includes that delivered through the solvent as well as that delivered directly to the chamber.

We demonstrate these two methods of controlling flow rate and vapor pressure using poly(methyl methacrylate) (PMMA) films swollen with toluene vapor. The films were prepared by spin-coating 3.4 wt. % solutions of PMMA (Sigma Aldrich, M_w = 350 000 g/mol) in toluene onto sample substrates (coverslip and QCM) at 2000 rpm. Prior to the swelling experiments, solvent vapors were equilibrated by bubbling carrier gas through the appropriate solvent reservoirs and bypassing the sample chamber for 30 min. In addition, the arm of the QCM was allowed to mechanically equilibrate for at least 2 h and parasitic capacitance was cancelled.

Initial film thickness was assessed via change of QCM frequency as described by Eqs. (1) and (2). Over nine samples, the change in resonance frequency of the QCM after spin-coating was 1427 ± 65 Hz, corresponding to film thickness of 213 ± 10 nm. This value was corroborated by subjecting a sample prepared in the same way to scratch analysis on an atomic force microscope (AFM), which yielded a thickness of 215 nm.

Swelling of the PMMA films with toluene vapor was then performed, varying either the toluene vapor pressure in the chamber or the mass flow rate of the toluene. First, nitrogen was bubbled through toluene in one channel, and a second channel was used to dilute the vapor with carrier gas. In these experiments, overall flow rate was kept constant at 100 sccm. Ultimate degree of swelling was expected to differ as the solvent vapor pressure varied with the mass flow of nitrogen through the solvent as described by Eq. (5). The expected behavior was observed, as was the fact that extent of swelling did not change linearly with partial toluene vapor pressure (Fig. 3, solid lines). This is in accordance with the previous studies that showed a non-linear decrease in the glass transition temperature for polymers undergoing vapor swelling, with the effect more dramatic at higher solvent weight fractions.[2]

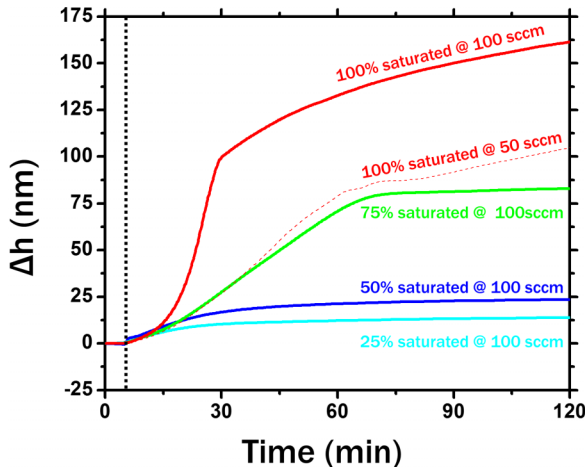

FIG. 3. (Solid lines) Change in film thickness (Δh) over time at various solvent partial vapor pressures attained by dilution from saturation. Data shown are for a total flow rate of Q_{nit} = 100 sccm. (Dotted line) Change in film thickness over time at saturated toluene vapor pressure at a total flow rate of Q_{nit} = 50 sccm. In both sets of data, temperature was held at 21 °C and vapor was introduced at 5 min (vertical dashed line).

Next, the rate of swelling was varied by controlling the solvent delivery rate. To accomplish this, a single channel was used to bubble nitrogen gas through toluene, and flow rate was varied. An example is shown in Fig. 3 for a scenario in which saturated toluene vapor was delivered at 50 sccm (red dotted line) compared to at 100 sccm (red solid line). This led to a slower rate of swelling, as expected.

In this set of experiments and similar experiments with different solvents that substantially swell the polymeric film, oscillations in apparent film thickness were sometimes evident. Visual observation of these samples after removal from the SVA chamber suggested that these oscillations were related to film de-wetting. Films studied here became susceptible to de-wetting under conditions in which the film swelled to greater than 1.5 times the initial film thickness, likely due to the solvent altering the surface-substrate interaction.[26,27]

B. Solvent mixtures

Mixtures of solvents are appropriate for some experiments, including attaining order in diblock copolymer films and preparing aggregates of conjugated polymers.[14,28,29] Such solvent mixtures can be delivered to a sample using either a solvent mixture in a single reservoir or pure solvents in separate reservoirs. We demonstrated ability to control and monitor vapor pressure in each scenario for a mixture of acetone and chloroform.

To demonstrate the expected dependence of vapor volume ratio on liquid volume ratio, mixtures of acetone and chloroform were prepared in a single solvent reservoir and flow rate was set at Q_{nit} = 100 sccm. The generated vapors were condensed at the solvent trap and subsequently analyzed by gas chromatography. The resulting liquid–vapor equilibrium curve for acetone-chloroform liquid solvent mixtures is shown in Fig. 4(a). The vapor volume ratio differs from the liquid volume ratio in accordance with the boiling points of each

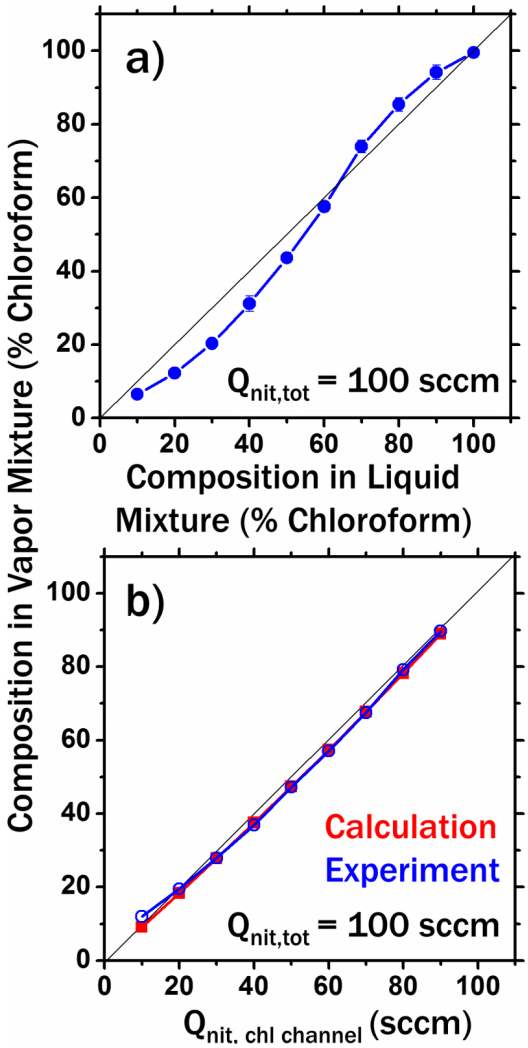

FIG. 4. (a) Liquid-vapor equilibrium curve for acetone-chloroform liquid solvent mixtures in a single reservoir. Error bars are standard deviations over 3 independent measurements, though most are smaller than the data points. (b) Experimental (blue) and calculated (red) chloroform vapor volume ratio as a function of Q_{nit} at the chloroform channel for acetone-chloroform solvent vapor mixtures with the two solvents in separate solvent reservoirs and $Q_{nit,tot}$ = 100 sccm.

solvent and their interactions, and the behavior seen is consistent with the previous reports.[30,31]

Mixed vapors can alternatively be prepared using separate solvent reservoirs. When acetone and chloroform are held in separate containers, the vapor volume ratio of each component can be straightforwardly controlled by varying the volumetric flow in each channel. For comparison with the results in Fig. 4(a), the total flow rate from both MFCs was held at 100 sccm. The calculated chloroform vapor volume ratio, based on Eqs. (3) and (4), agreed well with the experimental results (Fig. 4(b)).

Because partial vapor pressures are more easily controlled with separate solvent reservoirs, this configuration is recommended when employing a mixture of solvent vapors. However, this can be difficult and cost-prohibitive with non-binary mixtures that would require many MFCs. In this case, using mixed liquid reservoirs can be advantageous, though the vapor-liquid equilibrium would need to be characterized for the specific mixture of liquid solvents.

IV. SAMPLE DATA

A. Monitoring dynamics during polymer film swelling

The PMMA films depicted in Fig. 3 were monitored not only for film swelling with the QCM but also for film dynamics via imaging fluorescent dopants within the coverslip-mounted films. Such measurements were then used for subsequent particle tracking and analysis of diffusion constants across the film during the solvent swelling process.

The PMMA films were prepared as described above. For each experiment, one thin film was prepared on the QCM to characterize film thickness and swelling and another was prepared on a coverslip for imaging. The sample on the coverslip was doped with 3 nm CdSe/ZnS core-shell QDs (Ocean Nanotech, QSP-560-0050) at concentrations sufficiently low to achieve separation of ~2.5 μm between QDs.

Wide-field epi-fluorescence microscopy was employed to image the QD dopants to interrogate the dynamics of the film at various times during solvent swelling and as a function of position across the film. The motions of the QD dopants during film swelling are expected to reflect the dynamics and viscoelastic properties of the film. QD motions can be assessed and quantified following particle tracking, and the algorithm proposed by Crocker and Grier was used to identify and track the QDs in the sample data shown here.[32] From these tracks, mean-squared displacement (MSD) was then computed via

$$MSD = \langle \Delta r^2(\tau) \rangle = \left\langle [r\,(t+\tau) - r\,(t)]^2 \right\rangle,$$

where τ is the lag time and r is the particle's position. The MSD can be used to assess whether the tracked particles are undergoing diffusive behavior or anomalous diffusion including sub- or super-diffusive behaviors, which in turn can indicate caging effects or active transport, respectively. For diffusive behaviors, the MSD is directly related to the diffusion constant via $MSD = 2dD\tau$ with d the dimensionality of diffusion and D the diffusion constant. In particle-tracking microrheology, the MSD is also used to extrapolate local frequency-dependent storage and loss moduli.[23]

In the PMMA film before swelling, QDs are expected to be nearly immobile. Collecting data on ~45 QDs in such a dry film for 100 s and performing particle tracking on the resulting images showed that the ensemble average MSD over all QDs tracked resulted in a non-zero MSD (Fig. 5(a), black line). This effect is due to localization error[33–35] as was verified by a Monte Carlo simulation. To simulate the expected noise-related apparent motility, a point-spread function (PSF) matching that of experiment was generated at the center of a pixel array. Background intensity, signal-to-background ratio, and camera noise were applied as described previously.[36] A Gaussian fit was performed on the noisy PSF to determine centroid position before stochastic noise was renewed. This process was repeated 2700 times, and a MSD was constructed from the fitted positions, which will differ within localization accuracy. The MSD associated with the simulation is shown

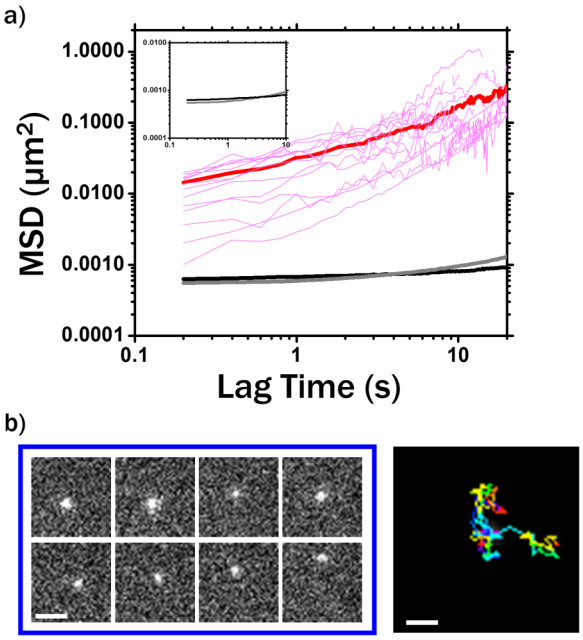

FIG. 5. (a) The MSDs of a subset of individual QDs tracked (thin red lines) in the swollen film, the ensemble average MSD (thick red line) from all tracked particles in the swollen film, the ensemble average of those in the as-cast film (black line), and a simulated ensemble MSD for immobile particles (gray line). Inset shows zoomed in MSDs for immobile particles (black) and simulation (gray). (b) (Left) Representative QD in the PMMA film swollen with 75% of saturated toluene vapor pressure at 21 °C (Fig. 3, green line). Fluorescence images have an exposure time of 0.2 s and were collected continuously. The images shown are each separated by 1 s. (Right) Positions of this QD shown over 75 frames (15 s) as obtained from particle tracking analysis. The QD is initially in the center of the frame. Time is indicated spectrally, with purple representing the earliest time points, and the images at left are from the blue portion of the trajectory. Scale bars are 1 μm.

in Fig. 5(a) (gray line), and it overlaps well with that obtained from the QDs in the dry film. This sets a lower bound on the diffusion constant that can be reliably obtained from this experiment at $\sim 10^{-5}$ $\mu m^2/s$.

Upon swelling of the PMMA with 75% of saturated toluene vapor pressure at 21 °C, the QD probes attained a degree of mobility due to rearrangement of the surrounding host polymer and/or QD diffusion in the free volume within the film. The motion of one such QD is shown in Fig. 5(b), along with a track depicting its motion over 8 s in the fully swollen film, as reported by the QCM trace. The MSD for this QD as well as several others (thin red lines) and the ensemble average of all QDs tracked (thick red line) are shown in Fig. 5(a). We note that some very fast QDs were not trackable due to the decrease in signal to background ratio that occurs when the photons emitted during the exposure time (0.2 s) are spread over a large area. The ensemble MSD was fit to a line yielding an average diffusion constant of the QDs in the film, $D = 5.2 \times 10^{-3}$ $\mu m^2/s$, consistent with expectation for a polystyrene film with ~30% mass solvent.[37] Importantly, the variation among individual QD MSDs suggests that the film is inhomogeneously mobile and that local viscoelasticity varies on the micron length scale in these swollen films. Particle tracking microrheology could then be used to characterize the variation in viscoelasticity as a function of position within the swollen film.

B. Monitoring and controlling aggregation during polymer film swelling

The multi-modal aspect of the SVA system was exploited to explore aggregation of single polymer chains in swollen films in real time. Here, poly(2-methoxy-5-(2-ethylhexyloxy)-1,4-phenylenevinylene) (MEH-PPV) synthesized as described previously[38] (M_w = 168 000 g/mol, PDI = 2.1) was embedded in PMMA (Sigma-Aldrich, M_w = 97 000 g/mol). Sample films were prepared by spin-coating a toluene solution of MEH-PPV containing 6.0 wt. % PMMA on the QCM sensor and the coverslip at ~2800 rpm for 60 s. The dried films had MEH-PPV concentration of $\sim 5 \times 10^{-7}$ M and were determined to have a thickness of ~270 nm via Eqs. (1) and (2). Change in film thickness over the course of SVA was calculated from measured change of mass per unit area of the film combined with known vapor volume ratio and independent measurements of film swelling with each of the two solvents to determine swelling capacity of the PMMA film with these solvents.

The sample films were then placed in the chamber and exposed to nitrogen gas flow at Q_{nit} = 400 sccm for 30 min to remove residual solvents. Following this, the films were swollen with solvent vapor using an acetone–chloroform solvent mixture in a single container. The liquid volume ratio was 50:50, resulting in a vapor volume ratio of 56.3%:43.7%, as shown in Fig. 4(a). Aggregates were prepared using two different solvent swelling conditions, one in which the acetone-chloroform mixture was delivered at saturated equilibrium vapor pressure and the one in which the vapor pressure was at 85% of the saturation level.

Polymer film swelling and aggregation of MEH-PPV molecules were monitored simultaneously. Figures 6(a) and 6(b) show degrees of film swelling as measured at the QCM together with wide-field fluorescence images taken of the sample during swelling. Since the fluorescence intensity of single chains is low compared to emission from aggregates, the illumination intensity (0.7 W/cm^2 at the sample) was chosen to best show the progression of aggregate formation rather than to allow visualization of single molecules.

Before solvent vapor exposure, the film exhibited moderate, largely homogeneous fluorescence as a result of many individual MEH-PPV chains dispersed within the film. The film was then swelled using the acetone-chloroform mixture as described above. Acetone is a selective solvent for the host PMMA matrix (having a Flory-Huggins interaction parameter of $\chi < 0.5$ for the host and $\chi > 0.5$ for MEH-PPV), thus swelling the host matrix allowing for diffusion of MEH-PPV chains. Mixing this solvent with chloroform, a non-selective good solvent for both MEH-PPV and PMMA, enables supersaturated conditions to be achieved and aggregation to be initiated.[28] Aggregation proceeds while the film is swollen as evidenced by decreasing intensity across most of the image alongside emergence of distinct bright features (Fig. 6(b)). This suggests that the onset of film swelling was accompanied by MEH-PPV chain diffusion that allowed the aggregation process to begin. In the fully swollen state, features become increasingly bright and their number decreases (Fig. 6(c)). This suggests that the growth of aggregates is

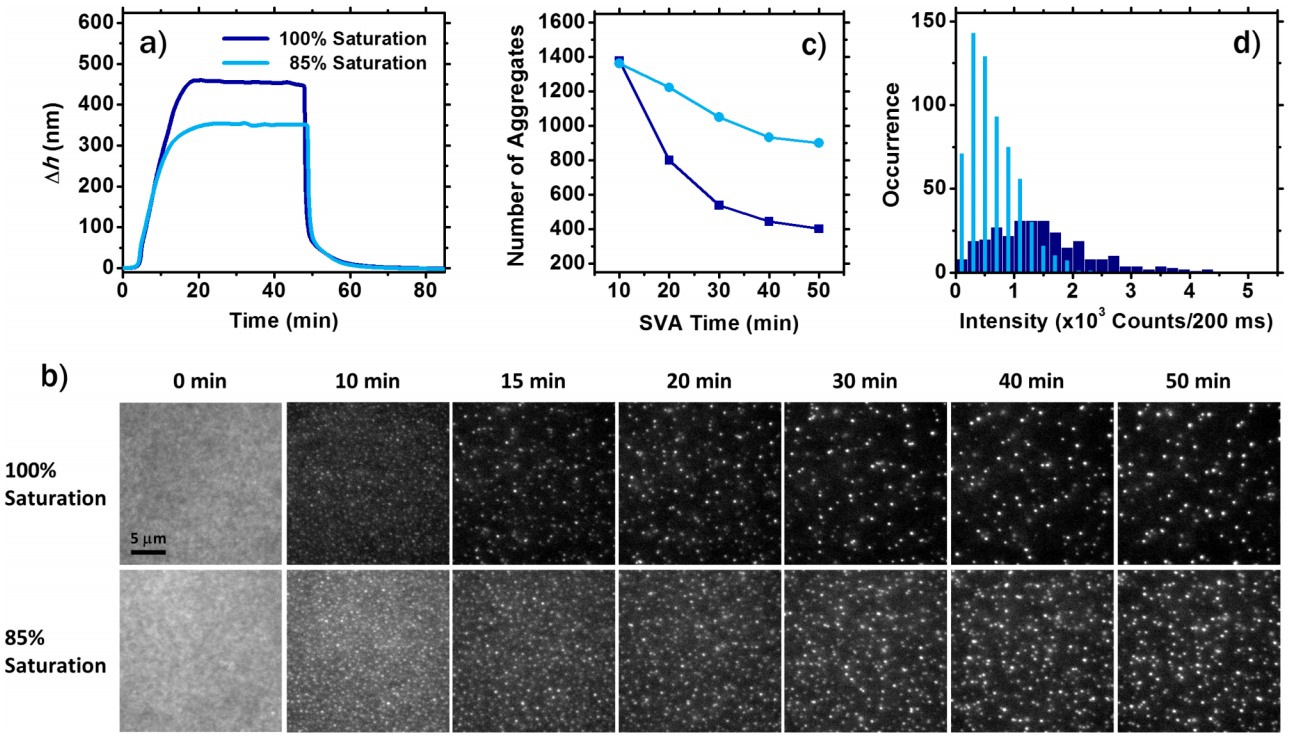

FIG. 6. *In situ* monitoring of aggregation of MEH-PPV polymers. (a) Degree of film swelling as a function of time for the sample films on the QCM sensor swollen with a 50:50 liquid volume chloroform:acetone mixture at 100% (dark blue) or 85% (light blue) saturated vapor pressure. (b) Wide-field fluorescence images and (c) number of fluorescent features found using feature finding algorithms adapted from Ref. 32 for films deposited on the coverslip at various points during the solvent vapor annealing process. Images represent ¼ of the total field of view used for feature finding and feature intensity quantification. Scale bar is 5 μm. (d) Histograms of average fluorescence intensity of individual aggregates obtained from films quenched with nitrogen gas after 50 min of solvent swelling. Median values are 1236 and 859 counts/200 ms for the films swollen at 100% and 85% saturated vapor pressure, respectively.

consistent with Ostwald ripening,[39–42] in which single polymer chains preferentially re-solvate from smaller aggregates and are incorporated into larger aggregates, as has been suggested previously.[28] While the two films have approximately the same number of aggregates 10 min into swelling, when the films are equally swollen, by 20 min it is evident that the film that is more swollen has fewer aggregates, suggesting that the aggregation process is limited by diffusivity of the single molecules and/or small aggregate species. While the degree of film swelling saturated after ~20 min of solvent vapor swelling, aggregate growth continued during the entire time the film was swollen, as judged by both the decreasing number of features and the increasing brightness of the imaged spots. Assuming the density of MEH-PPV chains is similar regardless of aggregate size, aggregate size will be correlated with fluorescence intensity.[28] Figure 6(d) shows histograms for the fluorescence intensity of individual aggregates after 50 min of solvent swelling of the film, with intensity calculated by averaging intensities of the 5 brightest pixels in each feature. Aggregates generated under the higher partial vapor pressure exhibited higher fluorescence intensity, reflecting their larger size. Such aggregates could be further characterized over the course of the swelling and de-swelling process by quantifying fluorescence intensity, fluorescence anisotropy, and/or emission spectra. These results, in which aggregates formed in a given time differ in size as a function of saturated vapor pressure delivered, hint at the prospect of controlling not only aggregate size but also photophysical properties such as fluorescence anisotropy and spectra through precise control of the solvent swelling process.

V. CONCLUSION

Solvent vapor annealing studies to date have been limited in their ability to simultaneously control and monitor extent of swelling while characterizing film microscopic structure and dynamics. We accomplish such control and measurement here by using mass-flow controllers to set solvent vapor pressures, a quartz crystal microbalance to characterize film swelling, and an epi-fluorescence microscope to characterize structure and dynamics within the film. This approach enables both the study of solvent vapor annealing processes and controlling the processes mediated by the solvent-swollen phases of polymer films.

ACKNOWLEDGMENTS

This work was supported in part by the National Science Foundation via a GRF for D.T.H. (No. DGE-11-44155) and NSF No. CHE 1213242.

[1]F. Muller-Plathe, Macromolecules **29**, 4782 (1996).
[2]T. S. Chow, Macromolecules **13**, 362 (1980).
[3]G. F. Billovits and C. J. Durning, Macromolecules **26**, 6927 (1993).
[4]J. S. Papanu, D. W. Hess, D. S. Soane, and A. T. Bell, J. Appl. Polym. Sci. **39**, 803 (1990).
[5]J. S. Papanu, D. S. Soane, A. T. Bell, and D. W. Hess, J. Appl. Polym. Sci. **38**, 859 (1989).

[6]P. Mansky, P. Chaikin, and E. L. Thomas, J. Mater. Sci. **30**, 1987 (1995).
[7]C. Sinturel, M. Vayer, M. Morris, and M. A. Hillmyer, Macromolecules **46**, 5399 (2013).
[8]G. De Luca, E. Treossi, A. Liscio, J. M. Mativetsky, L. M. Scolaro, V. Palermo, and P. Samori, J. Mater. Chem. **20**, 2493 (2010).
[9]J. Vogelsang and J. M. Lupton, J. Phys. Chem. Lett. **3**, 1503 (2012).
[10]D. R. Barbero and U. Steiner, Phys. Rev. Lett. **102**, 248303 (2009).
[11]K. R. Thomas, A. Chenneviere, G. Reiter, and U. Steiner, Phys. Rev. E **83**, 021804 (2011).
[12]Z. Y. Di, D. Posselt, D. M. Smilgies, and C. M. Papadakis, Macromolecules **43**, 418 (2010).
[13]X. D. Gu, I. Gunkel, A. Hexemer, W. Y. Gu, and T. P. Russell, Adv. Mater. **26**, 273 (2014).
[14]K. W. Gotrik, A. F. Hannon, J. G. Son, B. Keller, A. Alexander-Katz, and C. A. Ross, ACS Nano **6**, 8052 (2012).
[15]H. S. Lee, M. Q. Yee, Y. Y. Eckmann, N. J. Hickok, D. M. Eckmann, and R. J. Composto, J. Mater. Chem. **22**, 19605 (2012).
[16]A. Rao, S. H. Kang, B. D. Vogt, V. M. Prabhu, E. K. Lin, W. L. Wu, and M. Muthukumar, Langmuir **22**, 10009 (2006).
[17]S. Huttner, M. Sommer, A. Chiche, G. Krausch, U. Steiner, and M. Thelakkat, Soft Matter **5**, 4206 (2009).
[18]P. Mokarian-Tabari, T. W. Collins, J. D. Holmes, and M. A. Morris, ACS Nano **5**, 4617 (2011).
[19]E. Metwalli, J. Perlich, W. N. Wang, A. Diethert, S. V. Roth, C. M. Papadakis, and P. Muller-Buschbaum, Macromol. Chem. Phys. **211**, 2102 (2010).
[20]J. Q. Zhang, D. Posselt, A. Sepe, X. H. Shen, J. Perlich, D. M. Smilgies, and C. M. Papadakis, Macromol. Rapid Commun. **34**, 1289 (2013).
[21]A. Sepe, P. Cernoch, P. Stepanek, E. T. Hoppe, and C. M. Papadakis, Eur. Polym. J. **50**, 87 (2014).
[22]X. D. Gu, I. Gunkel, A. Hexemer, and T. P. Russell, Colloid Polym. Sci. **292**, 1795 (2014).
[23]D. Wirtz, Annu. Rev. Biophys. **38**, 301 (2009).
[24]G. Sauerbrey, Z. Phys. **155**, 206 (1959).
[25]K. K. Kanazawa and J. G. Gordon, Anal. Chem. **57**, 1770 (1985).
[26]G. Reiter, Phys. Rev. Lett. **68**, 75 (1992).
[27]K. M. Ashley, D. Raghavan, J. F. Douglas, and A. Karim, Langmuir **21**, 9518 (2005).
[28]J. Vogelsang, T. Adachi, J. Brazard, D. A. V. Bout, and P. F. Barbara, Nat. Mater. **10**, 942 (2011).
[29]Y. S. Jung and C. A. Ross, Adv. Mater. **21**, 2540 (2009).
[30]W. Reinders and C. H. De Minjer, Recl. Trav. Chim. Pays-Bas **59**, 369 (1940).
[31]W. Reinders and C. H. Deminjer, Recl. Trav. Chim. Pays-Bas **66**, 573 (1947).
[32]J. C. Crocker and D. G. Grier, J. Colloid Interface Sci. **179**, 298 (1996).
[33]R. E. Thompson, D. R. Larson, and W. W. Webb, Biophys. J. **82**, 2775 (2002).
[34]T. Savin and P. S. Doyle, Biophys. J. **88**, 623 (2005).
[35]D. S. Martin, M. B. Forstner, and J. A. Kas, Biophys. J. **83**, 2109 (2002).
[36]D. T. Hoang, K. Paeng, H. Park, L. M. Leone, and L. J. Kaufman, Anal. Chem. **86**, 9322 (2014).
[37]B. L. Hager and G. C. Berry, J. Polym. Sci., Polym. Phys. Ed. **20**, 911 (1982).
[38]C. J. Neef and J. P. Ferraris, Macromolecules **33**, 2311 (2000).
[39]W. Ostwald, Z. Phys. Chem. **22**, 289 (1897).
[40]I. M. Lifshitz and V. V. Slyozov, J. Phys. Chem. Solids **19**, 35 (1961).
[41]M. Kahlweit, Adv. Colloid Interface Sci. **5**, 1 (1975).
[42]R. D. Vengrenovitch, Acta Metall. **30**, 1079 (1982).